Journal of Alloys and Compounds 488 (2009) 442–447

Contents lists available at ScienceDirect

Journal of Alloys and Compounds

journal homepage: www.elsevier.com/locate/jallcom

Synthesis of different morphologies of bismuth sulfide nanostructures via hydrothermal process in the presence of thioglycolic acid

Masoud Salavati-Niasari[a,b,*], Davood Ghanbari[a], Fatemeh Davar[a]

[a] Institute of Nano Science and Nano Technology, University of Kashan, Kashan, P.O. Box 87317-51167, Islamic Republic of Iran
[b] Department of Chemistry, Faculty of Science, University of Kashan, Kashan, P.O. Box 87317-51167, Islamic Republic of Iran

ARTICLE INFO

Article history:
Received 19 August 2009
Accepted 27 August 2009
Available online 8 September 2009

Keywords:
Nanomaterials
Chemical synthesis

ABSTRACT

Different morphologies of bismuth sulfide (Bi_2S_3) nanostructures including nanoparticles, nanorods, nanobelts and nanoflowers have been prepared via a simple hydrothermal reaction between bismuth nitrate, $Bi(NO_3)_3{\cdot}5H_2O$, and thioglycolic acid (TGA) at relatively low temperature. Products were characterized by X-ray diffraction (XRD), scanning electron microscopy (SEM), transmission electron microscopy (TEM), ultraviolet–visible (UV–vis) spectroscopy, photoluminescence (PL) spectroscopy, Fourier transform infrared (FT-IR) spectra. The effect of reactant concentration, molar ratio of TGA to the bismuth nitrate, temperature and reaction time on the morphology, particle sizes and phases of nanocrystalline Bi_2S_3 products has been investigated.

1. Introduction

V–VI compound semiconductor materials have drawn much attention because of their excellent properties such as photoconductivity, photosensitivity, infrared (IR) spectroscopy and thermoelectric effect [1–5]. Among these materials, Bi_2S_3, owing to its high figure of merit (ZT) value, is widely used as a thermoelectronic-cooling material based on the Peltier effect [6]. It has a direct band gap material with Eg lying between 1.3 and 1.7 eV, which makes it useful in photodiode array and photovoltaic converters [7]. It also has application in television cameras, optoelectronic devices and IR spectroscopy [8].

Conventionally, Bi_2S_3 is prepared by the direct reaction of bismuth and sulfur vapor in a quartz vessel at high temperatures [9]. In the recent several years, many methods have been exploited to prepare nanostructured Bi_2S_3 with different morphologies, such as ultrasonic chemistry method [10], microwave-assisted route [11,12], photochemical synthesis method [13,14], high temperature thermal decomposition of single-source precursors [15,16], ionic liquid-assisted templating route [17], hydrothermal [18,19] and solvothermal methods [20–22]. However, most of the techniques mentioned above need relatively higher temperature and pressure, or the preparation procedures are complex. Therefore, it remains a challenge to develop a facile route to the fabrication of Bi_2S_3 nanomaterials in order to investigate its unusual properties, such as electrochemical applications.

Recently Yang et al. have developed a mild hydrothermal route to synthesize metal sulfides with the use of thioglycolic acids (TGAs) as nontoxic template [23]. And it is revealed that TGA acts as the oriented growth reactant during above process. We have presented a hydrothermal method, which is milder, simpler, more practical, and more environmental method than other methods. The trick in hydrothermal synthesis of star-like Bi_2S_3 nanocrystal presented here is the usage of thioglycolic acid (TGA) as a sulfur source and stability agents, which was previously used as the stability agent to prevent the chalcogenide nanocrystals from aggregating [24]. TGA has important roles in anisotropic growth of Bi_2S_3 crystals to rod-like nanostructure during the hydrothermal process. Comparative experiments show that TGA is capable of favoring the erosion reaction and inducing the orientation growth of the resultant metal sulfide nanocrystals [25].

We have been interested in the synthesis of CdS and ZnS nanostructures, using TGA, via hydrothermal method for a few years [26–28]. Addressing the above issue, we have used the TGA assisted hydrothermal process to successfully synthesize Bi_2S_3 nanostructures with different morphologies including nanoflower, nanorod and nanobelt, which may have wide potential applications in the future. We controlled the morphology and particle sizes of nanocrystalline Bi_2S_3 at 80–160 °C using bismuth nitrate and thioglycolic acid (TGA) as reactants in an aqueous solution. It was found that the molar ratio of TGA to Bi^{3+}, temperature and reaction time play key roles in controlling the morphology and particle sizes nanocrystalline Bi_2S_3.

* Corresponding author at: Institute of Nano Science and Nano Technology, University of Kashan, Kashan, P.O. Box 87317-51167, Islamic Republic of Iran.
Tel.: +98 361 5555333; fax: +98 361 5552935.
E-mail address: salavati@kashanu.ac.ir (M. Salavati-Niasari).

0925-8388/$ – see front matter © 2009 Elsevier B.V. All rights reserved.
doi:10.1016/j.jallcom.2009.08.152

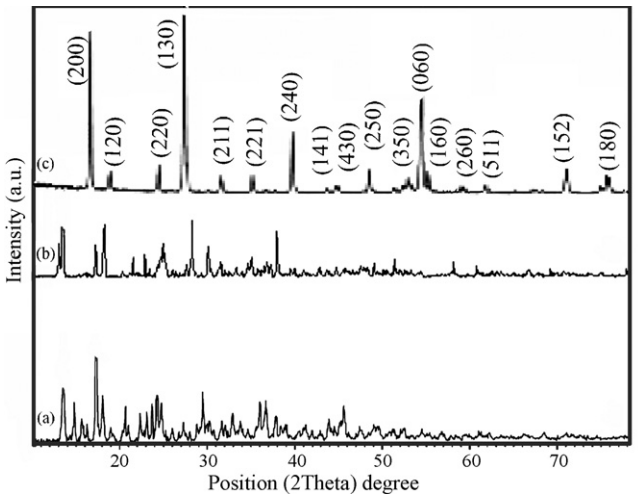

Fig. 1. XRD patterns of the Bi_2S_3 particles obtained for 5 h with 0.06 M TGA at (a) 80 °C, (b) 108 °C and (c) 160 °C.

2. Experimental

2.1. Materials and physical measurements

All the chemicals were of analytical grade and were used and received without further purification. XRD patterns were recorded by a Rigaku D-max C III, X-ray diffractometer using Ni-filtered Cu Kα radiation. Elemental analyses were obtained from Carlo ERBA Model EA 1108 analyzer. X-ray Photoelectron Spectroscopy (XPS) of the as-prepared products were measured on an ESCA-3000 electron spectrometer with nonmonochromatized Mg Kα X-ray as the excitation source. Scanning electron microscopy (SEM) images were obtained on Philips XL-30ESEM equipped with an energy dispersive X-ray spectroscopy. Transmission electron microscopy (TEM) images were obtained on a Philips EM208 transmission electron microscope with an accelerating voltage of 100 kV. Fourier transform infrared (FT-IR) spectra were recorded on Shimadzu Varian 4300 spectrophotometer in KBr pellets. The electronic spectra of the complexes were taken on a Shimadzu UV–visible scanning spectrometer (Model 2101 PC). Room temperature photoluminescence (PL) was studied on an F-4500 fluorescence spectrophotometer.

2.2. Preparation of Bi_2S_3 nanostructures

In a typical synthesis, 1.00 g (0.002 mol) of $Bi(NO_3)_3{\cdot}5H_2O$ powder is dissolved in 100 ml distilled water and 100 ml of 0.06 M thioglycolic acid which were mixed slowly under stirring. After stirring, the reactants were put into a 250 ml capacity Teflon-lined autoclave. The autoclave was maintained at 80–160 °C for 5–18 h and then cooled down to room temperature naturally. The product was centrifuged, washed with alcohol and distilled water for several times, and dried in oven at 50 °C for 10 h.

3. Results and discussion

The XRD patterns at the different temperatures showed that the crystallinities of the as-prepared products were continuously improving with increasing reaction temperature from 80 °C to 160 °C. Furthermore, a preferential orientation and a rod-like shape were observed in the sample obtained at 160 °C. The XRD pattern (Fig. 1a) of the synthesized product with TGA (0.06 M) for 5 h at 80 °C and 108 °C shows that the majority of the products were poorly crystallized and diffraction pattern matched with no JCPDS card No. When the reaction temperature increases from 80 °C to 160 °C, the crystallinity of the products will improve, as shown in Fig. 1b. The XRD pattern of as-prepared sample at 160 °C was indexed as a pure orthorhombic phase (space group *Pbnm*) which is very close to the values in the literature (JCPDS No. 17-0320 with cell constant $a = 11.1300$ Å, $b = 11.260$ Å, $c = 3.960$ Å). The strong and sharp reflection peaks in the XRD pattern indicated that Bi_2S_3 products were well-crystallized. The significantly intensified (2 0 0) peaks compared with the characteristic (1 3 0) diffraction peak of Bi_2S_3 reveal that there is a bias of orientations of the ⟨2 0 0⟩ crystallographic plane. The XRD patterns indicate that well-crystallized Bi_2S_3 products were obtained through the present hydrothermal synthetic route. The temperature was found to play a key role in the formation of nanocrystalline Bi_2S_3. The temperature also affects the particle sizes and morphology of Bi_2S_3 nanocrystals.

The SEM image in Fig. 2a shows that Bi_2S_3 powders obtained with TGA (0.06 M) for 5 h at 80 °C consist of irregular particles, whereas the product obtained at 108 °C for 5 h possesses a rod-

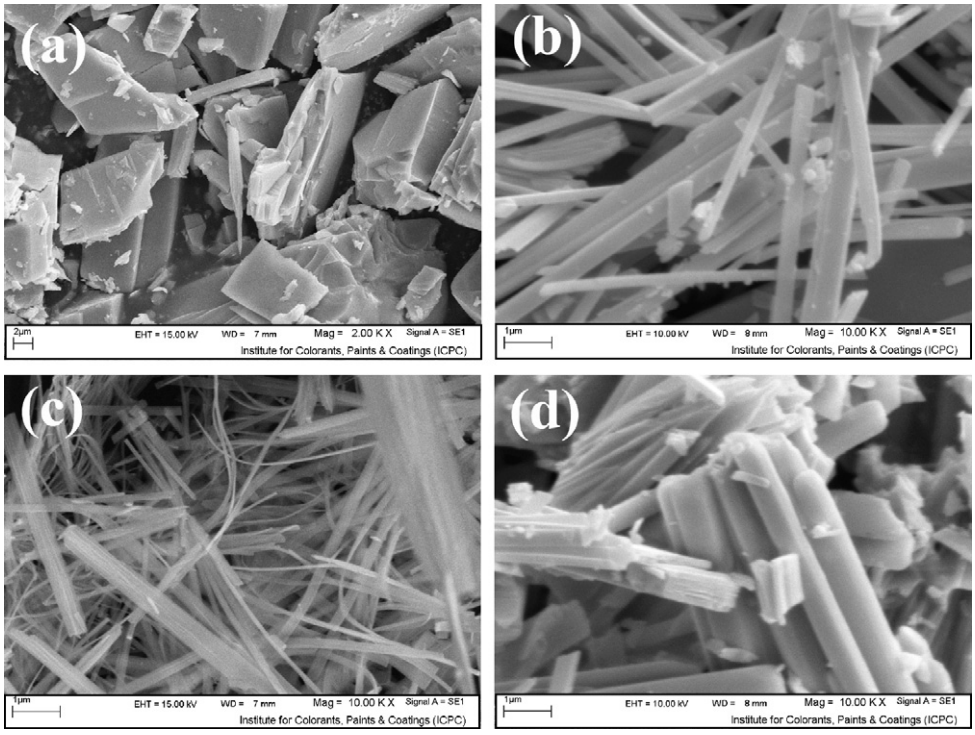

Fig. 2. SEM images of as-synthesized product with TGA 0.06 M for 5 h at (a) 80 °C, (b) 108 °C, (c) 160 °C and (d) 160 °C for 18 h.

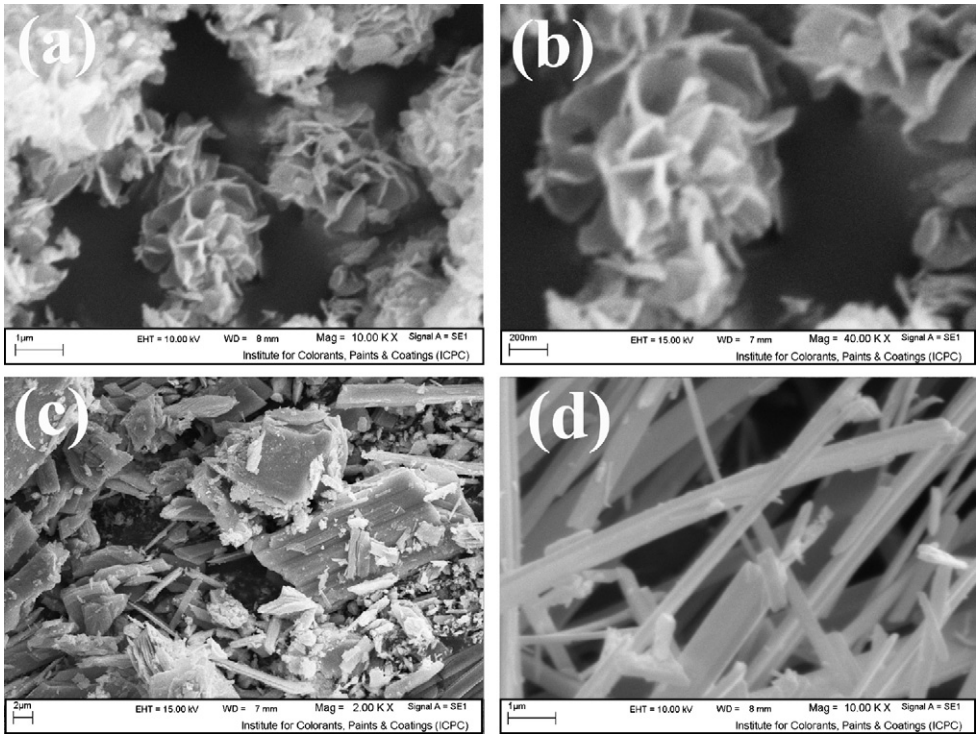

Fig. 3. SEM images of the as-synthesized product at 108 °C for 5 h at different concentration of TGA: (a and b) 0.02 M, (c) 0.04 M and (d) 0.06 M.

like Bi_2S_3 with diameter of 50–60 nm as shown in Fig. 2b. Upon raising the temperature to 160 °C, the product was found to consist of Bi_2S_3 nanobelt with widths ranging from 20 to 40 nm and lengths up to 10 μm (Fig. 2c). This illustrates that the nanoparticle size can be effectively controlled by setting the growth temperature. The effect of reaction time on the morphology and particle size of the products was investigated. As shown in Fig. 2d, when the reaction time was prolonged, from 5 to 18 h at 160 °C, morphology changes to a nanorod of increasing average diameter of 400–500 nm and length up to 4–5 μm. During preparation there is generally increasing particle size with time, which is consistent with an ostwald ripening process.

The effects of the Bi^{3+} to TGA mole ratio in the starting solution on the morphology and shape of Bi_2S_3 powders are shown in Fig. 3. In a series of experiments, the temperature was kept at 108 °C and the reaction time was 5 h. Fig. 3 shows the powder SEM images of the resultant products obtained with TGA:Bi^{3+} (1:1 to 3:1) at 108 °C for 5 h. With the increase in molar ratio, TGA:Bi^{3+}, from 1:1 to 3:1, morphologies of the as-synthesized Bi_2S_3 products change. In 0.02 M TGA (Fig. 3a) flower-like assemblies of nanosheets were formed (Fig. 3a). A high magnification image of a single cluster shown in Fig. 3b revealed the interpenetrating growth of some of the constituent nanosheets of the clusters. The widths of the individual sheets were of the order of 1 μm. Thickness of the individual nanosheets was less than 100 nm, but in 0.04 M irregular particles with some non-uniform microrod were observed (Fig. 3c). Upon increasing the TGA:Bi^{3+} mole ratio to 3, all the sample changes to nanorods with diameter of about 30–40 nm (Fig. 3d). This data indicates how reactant concentration could change the morphology of the product.

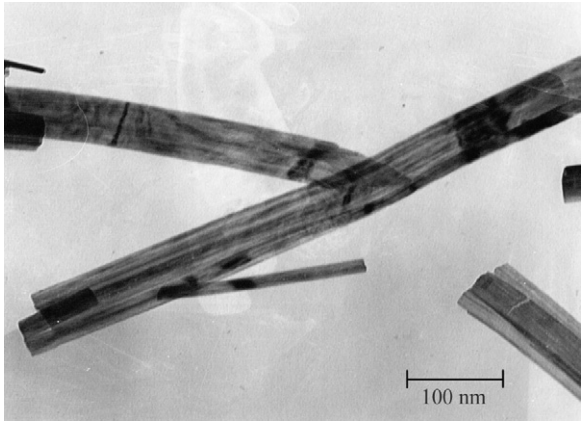

Fig. 4. TEM image of the Bi_2S_3 nanorod for 5 h with TGA (0.06 M) at 160 °C.

The typical TEM image of the Bi_2S_3 nanorods is indicated in Fig. 4. Bi_2S_3 nanorods with length varying from 0.5 to 1 μm can be seen in Fig. 4.

The purity and composition of the as-prepared sample are reflected by XPS analysis. No obvious impurities were detected in the XPS survey spectrum of Bi_2S_3 (Fig. 5a). The two strong peaks in Fig. 5b at 158.1 and 163.4 eV correspond to the Bi $4f_{7/2}$ and Bi $4f_{5/2}$, respectively, and the peak at 225.2 eV (Fig. 5c) can be attributed to the S (2s) binding energy. The XPS result coupled to the above XRD result further confirmed that pure Bi_2S_3 can be obtained under the current synthetic conditions [29].

The UV–vis absorption spectra of the as-synthesized Bi_2S_3 nanocrystals with different morphology were recorded as shown in Fig. 6. Compared with bulk Bi_2S_3, which has an absorption onset at 953 nm [30], the absorption edge of Bi_2S_3 nanostructures obtained here exhibit a large blue-shift, which is attributed to the quantum confinement of charge carriers in the nanoparticles [31]. It can also be seen that the absorption peak value of Bi_2S_3 nanobelts is smaller than those of other Bi_2S_3 nanostructures, indicating the smaller size of the Bi_2S_3 nanobelts.

Photoluminecsence (PL) measurement of Bi_2S_3 nanobelts was carried out at room temperature with excitation wavelength of 462 nm that is laid out in Fig. 7. The PL spectrum consists of one

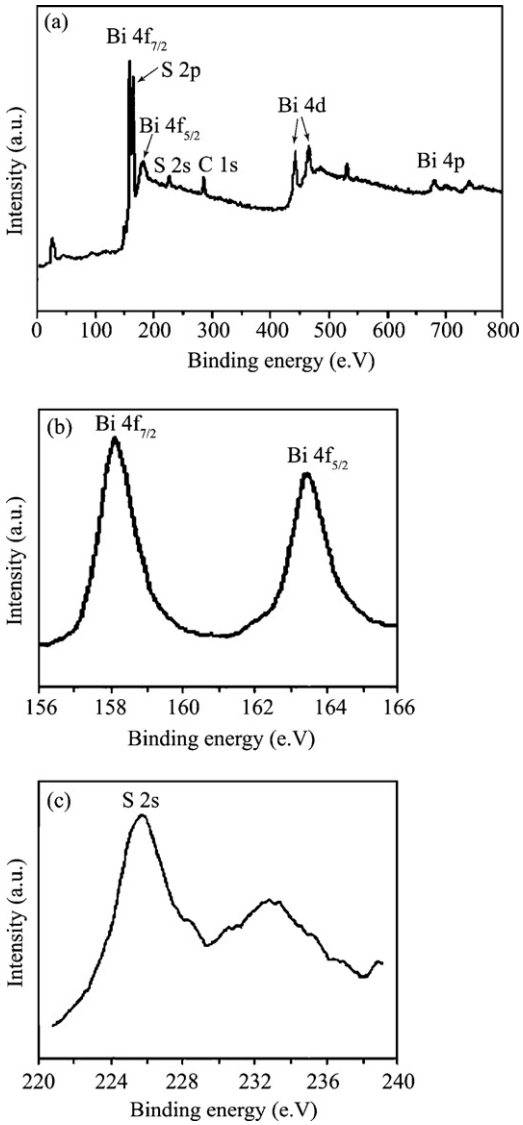

Fig. 5. XPS analysis of Bi_2S_3 nanobelts: (a) survey scan, (b) Bi region and (c) S region.

strong peak at 613 nm that can be ascribed to a high level transition in Bi_2S_3 semiconductor crystallites. It has been reported that this kind of band edge luminescence arises from the recombination of excitons and/or shallowly trapped electron–hole pairs [32].

The composition and quality of the product were analyzed by the FT-IR spectroscopy. Fig. 8 shows the FT-IR spectra of samples obtained. Curves (a) and (b) were the result of the sample obtained at 80 °C and 108 °C, respectively. In the curve (a), the typical absorbance at 3318, 2900, 2800 and 1550 cm^{-1} were revealed, which proved the presence of the thioglycolic acid at the sample [28]. Different from pure liquid-state thioglycolic acid, the IR vibration peaks of Bi_2S_3 obtained at 80 °C is much sharper and stronger, which signals weaker interactions and ordered arrangements of thioglycolic acid molecules existing in the reactant. This phenomenon could be explained by periodic intercalations of a relatively small amount of thioglycolic acid molecules into the inorganic frameworks composed of Bi_2S_3, which minimizes the interaction between neighboring thioglycolic acid molecules and results in fixed orientations of these thioglycolic acid molecules. In the IR spectra of Bi_2S_3 precursors, the stretching vibrations at frequencies above 3000 cm^{-1} related to pure thioglycolic acid shift towards lower frequency, which might result from the chemical bonding action between Bi^{3+}

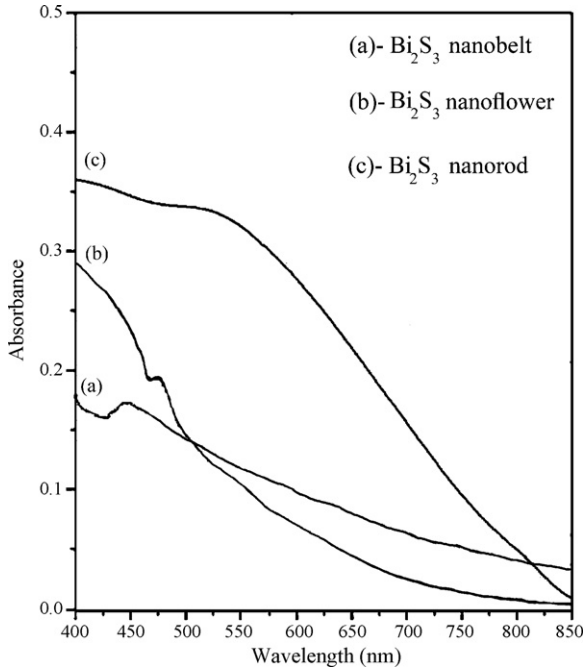

Fig. 6. UV–vis absorption spectrum of Bi_2S_3 prepared with (a) TGA (0.06 M) at 160 °C for 5 h (nanobelt), (b) TGA (0.06 M) at 108 °C for 5 h (nanorod) and (c) TGA 0.02 M at 108 °C for 5 h (nanoflower).

and S atom. In addition, at frequencies below 1600 cm^{-1}, the IR spectra of the Bi_2S_3 obtained at 80 °C exhibit many differences with the pure thioglycolic acid, which should be due to the ordered alignment and regular conformation of thioglycolic acid molecules in the precursors, while in liquid-state thioglycolic acid the orientation and conformation of the molecules are randomized due to thermal perturbation. On the other hand, for the curve (c), the corresponding bands intensity markedly disappears, so pure Bi_2S_3 sample was synthesized without any thioglycolic acid. Since Bi_2S_3 has no absorption peaks in the range of 4000–500 cm^{-1}

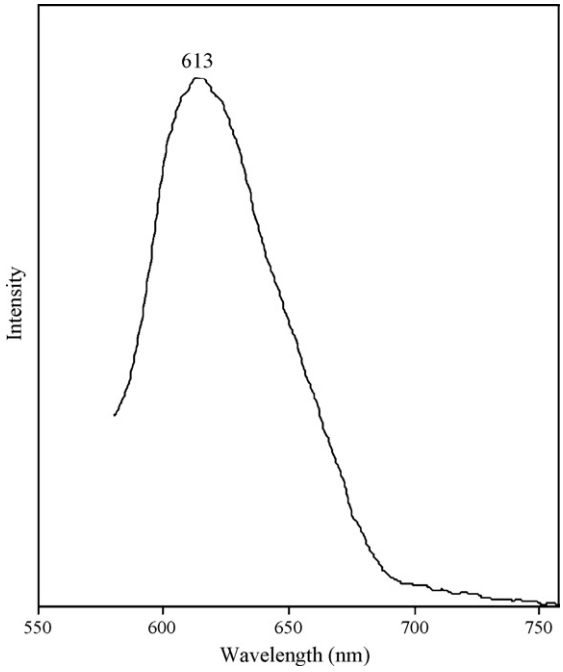

Fig. 7. Room temperature photoluminescence (PL) spectrum of Bi_2S_3 nanobelts.

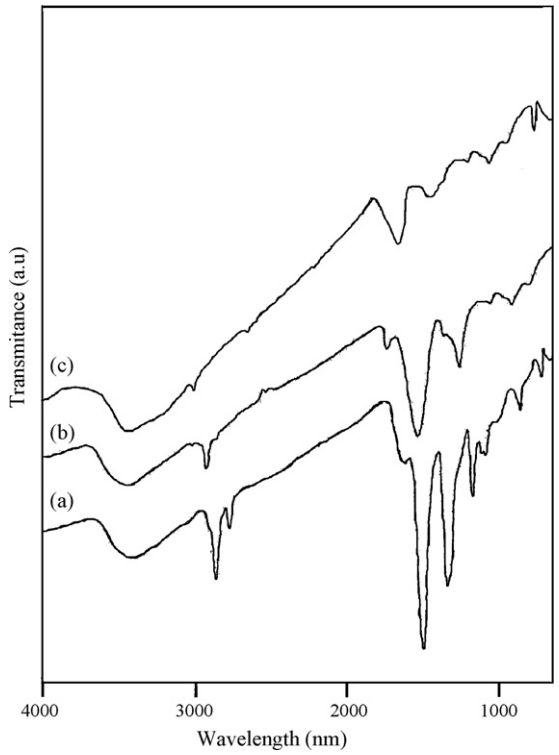

Fig. 8. FT-IR spectrum of as-synthesized products with 0.06 M TGA for 5 h at (a) 80 °C, (b) 108 °C and (c) 160 °C.

those peaks (positioned at 3318, 2900, 2800 and 1550 cm^{-1}) must be caused by the thioglycolic acid molecule absorbed on the surface of Bi_2S_3. We believe that these absorption peaks are close to those of $(Bi_2S_3)_m(BiSHCH_2COOH)_k^{2+}$ [33]. Considering all of these results, the whole process can be expressed as follows [33]:

$$3HSCH_2COOH + 2Bi^{3+} \longrightarrow Bi_2(HS)_3^{3+} + 3CH_2COOH^+$$

$$Bi_2(HS)_3^{3+} \longrightarrow Bi_2S_3 + 3H^+$$

$$mBi_2S_3 + kHSCH_2COOH + kBi^{3+} \longrightarrow (Bi_2S_3)_m(BiSCH_2COOH)_k^{2+} + kH^+$$

$$\downarrow$$

Complexed Bi_2S_3

According to above mechanism, the TGA acted as a 'soft template', leading to the anisotropic growth of Bi_2S_3 nanocrystals.

Previous report [33] suggests that the formation of Bi_2S_3 nanorods can be explained as follows: prior to the hydrothermal process, the dissociation of S^{2-} from TGA is significantly slow, and the formation of complexed Bi_2S_3 clusters, $(Bi_2S_3)_m(BiCH_2COOH)_k^{2+}$ is fairly limited. Meanwhile, during the hydrothermal process, the formation of $(Bi_2S_3)_m(BiCH_2COOH)_k^{2+}$, is remarkable due to the enhanced dissociation of S^{2-} from TGA at high temperature and pressure. In this case, it is invisible that the complexed Bi_2S_3 clusters aggregate somewhere because they are formed at a high rate. Therefore, Bi_2S_3 nanorod bundles were formed in this sample. Moreover, the growth of Bi_2S_3 nanorods with a preferential direction of *c*-axis can also be ascribed to its particular structure. Bi_2S_3 has a lamellar structure with linked Bi_2S_3 units forming infinite chains parallel to the *c*-axis [34]. The stronger covalent bond between the planes perpendicular to the *c*-axis facilitates higher growth rate along the *c*-axis (along the ⟨1 0 0⟩ orientation). The much weaker van der Waals bonding between the planes perpendicular to the *a*-axis limits the growth of the fiber in the horizontal direction and facilitates their cleavage to form one-dimensional nanostructures [35]. Prior to the hydrothermal process complexed Bi_2S_3 cluster i.e. $(Bi_2S_3)_m(BiSCH_2COOH)_k^{2+}$ were formed via above reactions. Here almost all the Bi^{3+} ions were complexed by TGA. But some residual Bi^{3+} ions transformed into Bi_2S_3 clusters. These Bi_2S_3 clusters would further be complexed by TGA giving negligible amount of Bi_2S_3 clusters prior to the hydrothermal process. Pure Bi_2S_3 nanorods were formed at the end of the reaction. There are Bi^{3+} ions exposed to the S^{2-} ions existing in the solution. Therefore formation of Bi_2S_3 proceeds along a certain direction giving specific shaped crystals. So the formation of Bi_2S_3 nanorods in the TGA assisted hydrothermal process is through cluster-to-cluster attachment mechanism. During the hydrothermal process, S^{2-} ions could be gradually dissociated from TGA. Therefore numerous Bi_2S_3 complexed clusters were generated during hydrothermal process. It is believed that the Bi_2S_3 nucleus is a microcrystal, therefore, strictly speaking, the bonding between the Bi_2S_3 nucleus and TGA is anisotropic. Accordingly, it is plausible that the dissociation of SCH_2COOH^- occurs at local regions of the complexed Bi_2S_3 clusters, where the Bi^{3+} ions exposed to the S^{2-} existing in the solution. Therefore, during the hydrothermal process, the formation of Bi_2S_3 proceeded along specific directions. In a way, the TGA acted as a 'soft template', leading to the growth of Bi_2S_3 nanobelts.

4. Conclusions

Nanocrystalline Bi_2S_3 with different morphologies and particle sizes was obtained via a simple hydrothermal reaction between $Bi(NO_3)_3{\cdot}5H_2O$ and thioglycolic acid (TGA). The effect of different parameters such as the molar ratio of TGA to Bi^{3+}, temperature, reaction time, which are known as the key parameter on the morphology and particle size of products were investigated.

Acknowledgment

Authors are grateful to Council of University of Kashan for providing financial support to undertake this work.

References

[1] G. Ghosh, B.P. Varma, Thin Solid Films 60 (1979) 61–65.
[2] D. Arivuoli, F.D. Gnanam, P. Ramasamy, J. Mater. Sci. Lett. 7 (1988) 711–713.
[3] L. Huang, P.K. Nair, M.T.S. Nair, R.A. Zingaro, E.A. Meyers, Thin Solid Films 268 (1995) 49–56.
[4] M.E. Rincón, P.K. Nair, J. Phys. Chem. Solids 57 (1996) 1937–1945.
[5] M.E. Rincón, R. Suárez, P.K. Nair, J. Phys. Chem. Solids 57 (1996) 1947–1955.
[6] H. Cui, H. Liu, X. Li, J. Wang, F. Han, X. Zhang, R.I. Boughton, J. Solid State Chem. 177 (2004) 4001–4006.
[7] B.B. Nayak, H.N. Acharya, G.B. Mitra, B.K. Mathur, Thin Solid Films 105 (1983) 17–24.
[8] D. Arivuoli, F.D. Gnanam, P. Ramasamy, J. Mater. Sci. Lett. 7 (1998) 711–714.
[9] C. Kaito, Y. Saito, K. Fujita, J. Cryst. Growth 94 (1989) 967–977.
[10] H. Wang, J.J. Zhu, J.M. Zhu, H.Y. Chen, J. Phys. Chem. B 106 (2002) 3848–3854.
[11] J. Lu, Q.F. Han, X.J. Yang, L.D. Lu, X. Wang, Mater. Lett. 61 (2007) 2883–2886.
[12] R. He, X. Qian, J. Yin, Z.K. Zhu, J. Cryst. Growth 252 (2003) 505–510.
[13] W.B. Zhao, J.J. Zhu, Y. Zhao, H.Y. Chen, Mater. Sci. Eng. B 110 (2004) 307–313.
[14] W.B. Zhao, J.J. Zhu, J.Z. Xu, H.Y. Chen, Inorg. Chem. Commun. 7 (2004) 847–850.
[15] X.P. Shen, G. Yin, W.L. Zhang, Z. Xu, Solid State Commun. 140 (2006) 116–119.
[16] G. Xie, Z.P. Qiao, M.H. Zeng, X.M. Chen, S.L. Gao, J. Cryst. Growth Des. 4 (2004) 513–516.
[17] J. Jiang, S.H. Yu, W.T. Yao, H. Ge, G.Z. Zhang, Chem. Mater. 17 (2005) 6094–6100.
[18] B. Zhang, X.C. Ye, W.Y. Hou, Y. Zhao, Y. Xie, J. Phys. Chem. B 110 (2006) 8978–8985.
[19] J. Ota, S.K. Srivastava, J. Phys. Chem. C 111 (2007) 12260–12264.
[20] W.J. Lou, M. Chen, X.B. Wang, W.M. Liu, Chem. Mater. 19 (2007) 872–878.
[21] H. Zhang, L.J. Wang, Mater. Lett. 61 (2007) 1667–1670.
[22] X.H. Yang, X. Wang, Z.D. Zhang, Mater. Chem. Phys. 95 (2006) 154–157.
[23] H. Zhang, D. Yang, S. Li, Y. Ji, X. Ma, D. Que, Nanotechnology 15 (2004) 1122–1125.
[24] A.M. Qin, Y.P. Fang, W.X. Zhao, H.Q. Liu, C.Y. Su, J. Cryst. Growth 283 (2005) 230–241.

[25] N. Gao, F. Guo, Mater. Lett. 60 (2006) 3697–3700.
[26] M. Salavati-Niasari, F. Davar, M.R. Loghman-Estarki, J. Alloys Compd. 481 (2009) 776–780.
[27] M. Salavati-Niasari, M. Reza Loghman-Estarki, F. Davar, Inorg. Chim. Acta 362 (2009) 3677–3683.
[28] M. Salavati-Niasari, M.R. Loghman-Estarki, F. Davar, J. Alloy. Compd. 145 (2009) 346–356.
[29] J. Lu, Q. Han, X. Yang, L. Lu, X. Wang, Mater. Lett. 61 (2007) 3425–3428.
[30] W. Li, Mater. Lett. 62 (2008) 243–245.
[31] M. Kowshik, W. Vogel, J. Urban, S.K. Kulkarni, K.M. Paknikar, Adv. Mater. 14 (2002) 815–818.
[32] J. Zhan, X. Yang, D. Wang, S. Li, Y. Xie, Y. Xia, Y.T. Qian, Adv. Mater. 12 (2000) 1348–1351.
[33] H. Zhang, Y. Ji, X. Ma, J. Xu, D. Yang, Nanotechnology 14 (2003) 974–977.
[34] J. Black, E.M. Conwell, L. Seigle, C.W. Spencer, J. Phys. Chem. Solids 2 (1957) 240–251.
[35] D. Wang, M. Shao, D. Yu, W. Yu, Y.T. Qian, J. Cryst. Growth 254 (2003) 487–491.